UNIVERSITY OF BIRMINGHAM
University of Birmingham Research at Birmingham

Continuous field estimation of dissolved organic carbon concentration and biochemical oxygen demand using dual-wavelength fluorescence, turbidity and temperature

Khamis, Kieran; Bradley, Christopher; Stevens, Rob; Hannah, David M.

DOI:
10.1002/hyp.11040

License:
Other (please specify with Rights Statement)

Document Version
Peer reviewed version

Citation for published version (Harvard):
Khamis, K, Bradley, C, Stevens, R & Hannah, DM 2017, 'Continuous field estimation of dissolved organic carbon concentration and biochemical oxygen demand using dual-wavelength fluorescence, turbidity and temperature', *Hydrological Processes*, vol. 31, no. 3, pp. 540-555. https://doi.org/10.1002/hyp.11040

Link to publication on Research at Birmingham portal

Publisher Rights Statement:
This is the peer reviewed version of the following article: Khamis, K., et al. "Continuous field estimation of dissolved organic carbon concentration and biochemical oxygen demand using dual-wavelength fluorescence, turbidity and temperature." Hydrological Processes (2016)., which has been published in final form at http://dx.doi.org/10.1002/hyp.11040. This article may be used for non-commercial purposes in accordance with Wiley Terms and Conditions for Self-Archiving.

Checked 8/11/2016

General rights
Unless a licence is specified above, all rights (including copyright and moral rights) in this document are retained by the authors and/or the copyright holders. The express permission of the copyright holder must be obtained for any use of this material other than for purposes permitted by law.

•Users may freely distribute the URL that is used to identify this publication.
•Users may download and/or print one copy of the publication from the University of Birmingham research portal for the purpose of private study or non-commercial research.
•User may use extracts from the document in line with the concept of 'fair dealing' under the Copyright, Designs and Patents Act 1988 (?)
•Users may not further distribute the material nor use it for the purposes of commercial gain.

Where a licence is displayed above, please note the terms and conditions of the licence govern your use of this document.

When citing, please reference the published version.

Take down policy
While the University of Birmingham exercises care and attention in making items available there are rare occasions when an item has been uploaded in error or has been deemed to be commercially or otherwise sensitive.

If you believe that this is the case for this document, please contact UBIRA@lists.bham.ac.uk providing details and we will remove access to the work immediately and investigate.

Download date: 17. Apr. 2024

Continuous field estimation of dissolved organic carbon concentration and biochemical oxygen demand using dual-wavelength fluorescence, turbidity and temperature

Khamis, K.[1,2*], C. Bradley[1] , R. Stevens[2], D.M. Hannah[1]

1. **School of Geography Earth and Environmental Science, University of Birmingham, Birmingham, B15 2TT, UK**
2. **RS Hydro Ltd, Leask House, Hanbury Road, Stoke Prior, Worcestershire, B60 4JZ, UK.**

*corresponding author: tel: +44 (0) 121 414 5557; e-mail: k.khamis@bham.ac.uk

ABSTRACT

Dissolved organic matter (DOM) quality and quantity is not measured routinely *in-situ* limiting our ability to quantify DOM process dynamics. This is problematic given legislative obligations to determine event based variability, however, recent advances in field deployable optical sensing technology provide the opportunity to address this problem. In this paper we outline a new approach for *in-situ* quantification of DOM quantity (Dissolved Organic Carbon: DOC) and a component of quality (Biochemical Oxygen Demand: BOD) using a multi-wavelength, through-flow fluorescence sensor. The sensor measured tryptophan-like (Peak T) and humic-like (Peak C) fluorescence, alongside water temperature and turbidity. Laboratory derived coefficients were developed to compensate for thermal quenching and turbidity interference (i.e. light attenuation and scattering). Field tests were undertaken on an urban river with ageing wastewater and stormwater infrastructure (Bourn Brook; Birmingham, UK). Sensor output was validated against laboratory determinations of DOC and BOD collected by discrete grab sampling during baseflow and stormflow conditions. Data driven regression models were then compared to laboratory correction methods. A combination of temperature and turbidity compensated Peak T and Peak C was found to be a good predictor of DOC concentration ($R^2 = 0.92$). Conversely, using temperature and turbidity correction coefficients provided low predictive power for BOD ($R^2 = 0.46$ and $R^2 = 0.51$, for Peak C and T respectively). For this study system, turbidity appeared to be a reasonable proxy for BOD, $R^2 = 0.86$. However, a linear mixed effect model with temperature compensated Peak T and turbidity provided a robust BOD prediction ($R^2 = 0.95$). These findings indicate that with careful initial calibration, multi-wavelength fluorescence, coupled with turbidity and temperature provides a feasible proxy for continuous, *in-situ* measurement of DOC concentration and BOD. This approach represents a cost effective monitoring solution, particularly when compared to UV- absorbance sensors and DOC analysers, and could be readily adopted for research and industrial applications.

Keywords: Water quality, optical sensors, in-situ monitoring, urban river systems.

INTRODUCTION

Recent advances in field deployable instrument technology have enabled an increase in the scope and resolution of water quality monitoring in freshwater systems (Wade *et al.*, 2012; Strohmeier *et al.*, 2013; Outram *et al.*, 2014; Bieroza and Heathwaite, 2015). In particular, fine scale resolution data (sub daily - sub hourly) demonstrates that conventional sampling regimes, which are often used by environmental regulators and researchers (i.e. weekly time step and reliant on grab samples), fail to represent adequately catchment water quality dynamics (Cassidy and Jordan, 2011). This is particularly pronounced in systems with parameters that display marked diurnal periodicity (Halliday *et al.*, 2015). This deficiency of conventional sampling campaigns has significant implications for our understanding of water quality process dynamics. Moreover, it highlights the need for better informed sampling strategies for regulatory monitoring purposes (Halliday *et al.*, 2015).

To date, most high resolution, *in-situ* water quality monitoring studies have focused on rural river catchments (Outram *et al.*, 2014). The study of urban river systems using field deployable sensors or analyzers has been relatively neglected, despite their prevalence and the significant water quality problems associated with urban rivers (Viviano *et al.*, 2014; Halliday *et al.*, 2015). Here, organic pollution (point source and diffuse) is a key concern and labile dissolved and particulate organic matter (OM) is supplied to the channel from numerous sources and pathways leading to increased microbial loading (Ouattara *et al.*, 2014), eutrophication and depletion of dissolved oxygen (Halliday *et al.*, 2015). Dissolved Organic Carbon (DOC) concentration is widely used as an indication of the dissolved fraction (DOM) and provides an indication of quantity but no information on quality, such as lability (Fellman *et al.*, 2008). Biochemical Oxygen Demand (BOD), a laboratory measurement of the oxygen required for aerobic oxidation of labile carbon in a water sample, is widely used as an indicator of both particulate and dissolved organic pollution (Jouanneau *et al.*, 2014). Many governments and large industries have monitoring obligations with thresholds and environmental permits often set based on oxygen requirements for fish survivorship (Collins and Voulvoulis, 2014).

In lowland rivers a large proportion of BOD is thought to be particulate (Sullivan *et al.*, 2010) and associated with degraded phytoplankton cells (Volkmar and Dahlgren, 2006). In urban rivers generally, BOD is highly variable and largely driven by storm water dynamics (Lee

and Bang, 2000) and associated particulate transport (sediment/biofilm associated organic material and microbes) from impervious surfaces, storm drains and deposited sediments (Sakrabani *et al.*, 2009; Kim and Sansalone, 2010). Given the diversity of OM sources within urban catchments (Goldman *et al* 2012; McElmurry *et al.*, 2014) robust *in-situ* or real-time monitoring methods are required to improve: (i) process understanding (e.g. climate – source – pathway); (ii) legislative monitoring capacity; and (iii) assessment of river restoration initiatives (Khamis *et al.*, 2015).

Recent advances in optical techniques offer a promising solution with the potential to monitor DOC and BOD concentrations *in-situ*. For example, absorbance in the UV or visible spectrum (e.g. at 254nm), has been widely used as a DOC surrogate (Peacock *et al.*, 2014) and field deployable sensors that measure the UV spectrum (i.e. 200 - 500nm) have yielded good relationships between field and laboratory data (Sandford *et al.*, 2010; Strohmeier *et al.*, 2013; Jones *et al.*, 2014). However, these sensors are expensive and this has hitherto limited the development of multi-node networks for high resolution spatial monitoring of DOC concentration. *In-situ* UV fluorescence sensors measuring humic-like fluorescence (Peak C; $\lambda_{excitation.} = 365$ nm $\lambda_{emission} = 470$ nm), also referred to as fluorescent organic matter (FDOM), generally have a lower unit cost than UV absorbance sensors and their signal output appears to correlate strongly with DOC concentration once turbidity and temperature interference are corrected (Saraceno *et al.*, 2009; Downing *et al.*, 2012).Yet to-date, application of this technology has been limited to rural catchments and urban river systems appear to have been largely neglected with a distinct bias towards North American systems (Pellerin *et al.*, 2011; Downing *et al.*, 2012; Carpenter *et al.*, 2013; Etheridge *et al.*, 2014).

To-date few studies have explored *in-situ* BOD measurement using optical surrogates, although laboratory based studies have highlighted the potential for absorbance (Comber et al., 1996) and fluorescence based surrogates of BOD (Hudson *et al.*, 2008; Yang *et al.*, 2014). Xu and Xu (2015) outlined the suitability of *in-situ* fluorometery (Chlorophyll a, $\lambda_{excitation} = 460$, $\lambda_{emission} = 685$) to monitor BOD in a eutrophic lake system, although they measured the response to elevated labile OM (i.e. phytoplankton abundance) rather than determining the labile OM concentration directly. Tryptophan-like fluorescence (Peak T, $\lambda_{excitation} = 280$ nm, $\lambda_{emission} = 350$ nm) is correlated strongly with reactive OM, and is thought to represent a mixture of dissolved proteinaceous material and polyphenolic compounds (Yamashita and

Tanoue, 2003; Beggs and Summers 2011; Aiken, 2014). In the laboratory Peak T has been correlated with BOD (Hudson *et al.*, 2008) and microbial abundance (Cumberland *et al.*, 2012). However, as mentioned above, most BOD is in the particulate fraction and thus some of the challenges associated with fluorescence based DOC monitoring (e.g. turbidity interference and temperature quenching) are difficult to overcome. Turbidity correction in particular poses a particular problem as filtering will remove the particulate fraction (Saraceno et al., 2009) and laboratory derived correction factors (e.g. Downing et al., 2012; Khamis et al., 2015) are only suitable for quantification of the dissolved fraction. Hence, field based calibrations may be necessary to construct robust, data driven regression models to estimate BOD from multiple *in-situ* optical sensors.

A multi-wavelength fluorescence sensor platform (Peak C and Peak T) has the potential to address some of the research gaps outlined above, and yield high resolution information on DOM quantity (DOC concentration) and OM quality (BOD concentration). The aim of this study was to validate and refine a new cost effective monitoring system offering continuous quantification of BOD and DOC concentration using multi-wavelength fluorescence measurements, alongside turbidity and temperature to correct for confounding environmental interferences (Downing *et al.*, 2012; Khamis *et al.*, 2015). In undertaking this study, we also sought to address the specific challenges of monitoring DOM in urban river systems, particularly the accurate quantification of stormflow organic loads. We hypothesised that a combination of measurements, Turbidity, Peak T and C, would provide a better estimation of BOD and DOC concentration that single parameters. More specifically we sought to test the suitability of laboratory derived compensation coefficients in an urban systems with a responsive hydrology.

METHODS

Sensor characteristics, calibration and compensation

A GGUN - FL30 fluorometer (Albillia Co, Neuchatel, Switzerland) was used in the field trial. The sensor was initially designed for tracer tests (Lemke *et al.*, 2013), but was modified to monitor DOM (Peak T and Peak C; see Fig. 1 and Table 1) and turbidity. Briefly, the sensor comprises a pyrex flow cell housed in a stainless steel case (d = 0.16 m; h = 0.17 m) with optical components installed along two orthogonal axes (Fig. 1a). The instrumentation

components include: (i) an excitation branch (LED, filter and condenser lens) and, perpendicular to this, (ii) a detection branch (lens, filter and photodiode). The LEDs, filters and photodiodes were selected to match the spectral properties of the DOM peak of interest (Fig 1b). For Peak T the selected excitation wavelength (285 nm) differed from the commonly reported maximal excitation for Peak T (270-280 nm; Fellman *et al.*, 2010) this was due to: (i) previous research on urban river systems highlighting the importance (in urban rivers) of the peak at 282 ± 3nm (Baker, 2005); (ii) high current draw, low optical output and decreased lifetime of lower UV LEDs, and; (iii) comparability with other *in-situ* Peak T fluorometers (i.e. Turner Cyclops 7). The sensor has an integrated thermistor (sensitivity = 0.01 °C) attached to the inside of the pyrex tube to monitor sample temperature, and enable quantification (and correction) of the thermal quenching of the fluorescence signal (Baker, 2005; Watras *et al.*, 2011). A small peristaltic pump (Model 810, Williamson Pumps Ltd, Poynings, UK**)** was attached to the sensor with silicon tubing to facilitate sample collection.

Sensor calibration was undertaken in a temperature controlled laboratory (20 °C), pre and post deployment, to assess drift due to electronics/optics. For each of the three optical parameters a 6 point dilution series was created (0 – 1000 ppb for Peak T and C; and 0 -1000 FNU for turbidity): (i) Peak C (quinine sulphate dehydrate dissolved in 0.05 M $H_2 SO_4$); (ii) Peak T (L- tryptophan dissolved in ultra-pure water; Milli-Q, 18.2 $M\Omega^{-1}$), and; (iii) turbidity (using a suspension of formazine). For each measurement concentration, the sensor was allowed 1 min to stabilize before logging 10 readings every 10 s. Detection limits, precision, accuracy and linear range were determined following Pellerin *et al.*, (2013). However, for clarity and comparability with other published work (Baker, 2004; Watras *et al.*, 2011) the voltage output (mv) of the sensor, referred to as relative fluorescence units (RFU) herein, is reported for Peaks T and C.

Temperature quenching was tested in the laboratory using water collected from the study site (see Fig. 1). River water from the study site (DOC = 3.7 ± 0.2 mg L^{-1}) was mixed with ultra-pure water to create a 4 point dilution series (1, 0.75, 0.5, 0.25). Solutions were kept in a temperature controlled dark room (5 °C) for 24 h before experiments were undertaken. For each concentration 1 L was placed in a 2 L glass beaker and transferred to a MLR-352, 294L programmable incubator (Sanyo, Osaka, Japan). The sensor and pump system were placed in the incubator and warmed (5 – 20 °C) over a period of 6 h (mean rate of change = 2.5 °C h^{-1}) logging readings at 3 min resolution (CR 1000; Campbell Scientific). A linear correction

model (similar to that commonly used to correct EC data) was applied to provide peak T and C fluorescence intensity standardised to 20 °C (see Khamis *et al.*, 2015). Briefly, Ordinary Least Squares (OLS) regression was applied to the data and ρ, the temperature compensation factor, was calculated as the ratio of the slope to the intercept at 20°C (slope/intercept$_{20°C}$). Data were then corrected using:

$$F_{ref} = \frac{F_{mes}}{1 + \rho(T_{mes} - T_{ref})} \qquad (1)$$

where F is the fluorescence signal (i.e. Peak T or Peak C), T is temperature (°C) and subscripts *mes* and *ref* represent the measured and reference values respectively. Following previous studies a reference temperature of 20°C was chosen, thus T_{ref} = 20°C and F_{ref} represents the fluorescence signal at 20°C. Herein temperature corrected fluorescence will be denoted with a subscripted 20 (e.g. Peak T_{20}).

To assess the effect of turbidity on the sensor readings three sediment types were used: (i) clay/fine silt (D_{50} = 11.9 µm); (b) coarse silt (D_{50} = 52.1 µm) and (c) river sediment from the study site (fine sand; D_{50} = 82.1 µm). Following Khamis et al. (2015) all sediments were treated with 30% hydrogen peroxide (H_2O_2) to remove organic material and were thoroughly rinsed in ultra-pure water. River water samples (1 L) were then transferred to a 2 L glass beaker and constantly stirred on a magnetic stir plate. Weighed sediment was added incrementally to give a range of turbidity comparable to that likely to be observed in the field (i.e. 0 – 500 FNU) and a range in which correction algorithms are still robust (i.e. before an asymptote is reached). For each increment water was pumped through the sensor and 10 readings were taken. Sensor readings were then corrected based on the sediment regression model for the study site following methods outlined by Downing et al. (2012).

Site description

The sensor was deployed on the Bourn Brook, a tributary of the River Rea, Birmingham, UK (52°27'N, 1°54'W; Fig. 2 a&b). Monitoring was conducted during spring 2015 (27th March - 8th June 2015). A detailed description of the basin is provided by Carstea *et al.* (2009): briefly, the catchment is 27.9 km^2 and urban or suburban land use extends over ~80% of the basin (Morton *et al.*, 2011; Fig 2c). There are no wastewater treatment works within the catchment; but an extensive, ageing (>100 years) network of storm sewers and combined

sewer overflows discharge to the main channel. Hence, the system is particularly dynamic ('flashy') in terms of both river flow and DOM fluxes (Carstea *et al.*, 2010). Catchment elevation ranges from 116 m, at the catchment outlet, to 234 m in the headwaters where there is a limited area of woodland (< 10 % of total catchment area) (Fig 2c). At the monitoring location the stream is 3.1± 0.2 m wide and at base flow has a mean depth of 0.18 ± 0.08 m.

Field monitoring and sampling

The FL30 fluorometer was deployed on the river bank to facilitate maintenance and avoid instrument damage. Water was abstracted from the stream using a peristaltic pump (Model 810, Williamson Pumps Ltd, Poynings, UK) and passed through an inlet strainer (250 µm mesh screen) located ~0.05 m above the stream bed, before flowing through 3 m of silicon tubing (6 mm ID) and the FL30 flow cell before being returned to the river. The pump was controlled using a CR 1000 data logger (Campbell Scientific, Logan, USA) and relay switch. A 5V pulse activated the pump for 3 mins. every hour, to flush the system with sample water. At hourly intervals 5 readings of all parameters were taken at 10 s intervals and their mean logged. An integrated water temperature/electrical conductivity probe and a vented pressure transducer (see Table 1 for specifications) were located in the channel and measurements logged at 3 min. intervals. A stage – discharge relationship ($R^2 = 0.98$, data not shown) was created using the velocity-area method (Herschy, 1985).

Given the sensor design, it was not feasible to include an automated cleaning function using compressed air or a mechanical wiper. Thus, the pyrex measurement chamber was cleaned manually at weekly intervals with ultrapure water and a soft brush. Step changes in fluorescence output were observed post cleaning for Peak C (mean ± SD; -15.2 ± 2.1 %) and Peak T (-17.4 ± 2.7 %) and logged data were subsequently corrected using a linear regression model assuming a consistent rate across all timesteps (Conmy *et al.*, 2014). Further, to inhibit biofilm development in the pump tubing, the FL30 system was flushed with 10% hydrochloric acid (HCl) and ultrapure water every two weeks.

On four occasions when high flow conditions were anticipated, 1 L river water samples were collected at 1 h intervals. The aim was to capture pre-event baseflow, rising limb, peak flow and falling limb conditions for each event. All samples were collected using a refrigerated, automatic pump sampler (Avalanche, ISCO, Lincoln, USA), retained in acid washed bottles and returned to the Water Sciences laboratory at the University of Birmingham for analysis within 12 h of collection.

A further spatial sampling sweep was conducted to collect samples from locations representative of potential watersources within the catchment. Bulk samples were collected from 4 sites: (i) the Bourn Brook (3.58 mg L^{-1}, 5.2 FNU); (ii) the Worcester and Birmingham canal (4.02 mg L^{-1}, 15.3 FNU); (iii) a storm drain in the Bourn Brook catchment (7.28 mg L^{-1}, 10.6 FNU), and; (iv) the settled sewage tank at a local sewage treatment works (Bromsgrove, Worcestershire, UK) (18.13 mg L^{-1}, 175.4 FNU). Samples were diluted with ultrapure water to create a dilution series representing sample volumes (100%, 75%, 50%, 25%, 12.5%) and measurements made with the FL30. A further suite of laboratory analysis was undertaken on each sample as detailed below.

Analytical procedure and data processing

In the laboratory 0.25 L of each sample was filtered through Whatman GF/G filter papers (pore size 1.2 µm) that had been pre-rinsed in HCI and ultrapure water. The pore size was chosen following Baker *et al.*, (2007) as a trade-off between optical clarity (removal of the high sediment loads associated with storm event samples) and obtaining a sample that could be compared to the BOD measurement. Prior to analysis, all samples (filtered 0.25 L and unfiltered 0.75 L) were raised to 20 °C in a water bath. BOD analysis was then conducted on the unfiltered water sample following ISO 5815-1:2003 (ISO 5815-1:2003, 2003). For the filtered component, DOC was determined using a Shimadzu TOC-V CSH total organic carbon analyzer (Kyoto, Japan). For each sample, replicate DOC readings (n = 3-5) were undertaken and ≤ 2% coefficient of variation was observed. UV – Visible absorbance spectra (200 – 850nm; cuvette path length 10 mm) were collected using a Jenway 6800 dual beam spectrophotometer (Stone, UK). Measurements were completed using a quartz cuvette that had been triple rinsed with sample water prior to the analysis.

Laboratory fluorescence measurements were undertaken using a Cary Eclipse Spectrofluorometer (Varian Inc., Palto Alto, USA) with instrument settings outlined in Khamis *et al.* (2015). Following Lawaetz and Stedmon (2008), a Raman blank was measured at the start of each instrument run and used to calibrate fluorescence intensity. Excitation Emission Matrices (EEMs) were determined for each sample (plus an ultrapure water blank) over the excitation range of 200 - 400 nm (5 nm slit width) and emission range of 280 – 500 nm (2 nm slit width). Samples with high OM concentrations (absorbance 254nm > 0.3 AU) were diluted

with ultrapure water before analysis. EEMs were pre-processed in Matlab (version 2011a) using the drEEM toolbox, following Murphy *et al.* (2013). A user-developed peak picking algorithm was used to extract Peak T (Ex: 285 nm and Em: 345 nm) and Peak C (Ex: 365 nm and Em: 490 nm) intensity, a further algorithm was used to identify the maximal location of peak T and C.

Statistical analysis

Linear mixed effect models (LMMs) were employed to investigate relationships between *in-situ* measurements and response variables of interest (i.e. laboratory measurements of BOD and DOC). All models consisted of a fixed component comprising the predictor variables; Peak C, Peak T, Peak C_{20} and Peak T_{20}, turbidity corrected Peak C_{20} and Peak T_{20} and turbidity. Storm event was included as a random component to control for the nested sampling structure (i.e. sample within event) and both the slope and intercept could vary between events. Model residuals were inspected and temporal auto-correlation was identified. Hence, an AR1 correlation structure was incorporated in the final model. We conducted the same procedure for the dataset with all samples >100 FNU removed to assess the influence of high turbidity events on the empirically derived correction factors and data driven regression model. All LMMs were ranked by AICc scores (Burnham and Anderson, 2002). R^2 values were calculated following Nakagawa and Schielzeth (2013) and along with, mean absolute error (MAE) and percent bias (% bias), were used to evaluate goodness of fit between observed and modelled DOC and BOD (Moriasi *et al.*, 2007). All LMMs were fitted using the nlme package in R version *2.15.2* (R Development Core Team, 2012).

RESULTS AND DISCUSSION

Sensor calibration and performance

Sensor calibration and laboratory testing identified a linear range for Peak T (L-Tryptophan standard) and Peak C (quinine sulphate standard) across a 0 – 1000 ppb concentration range (Table 1; Supplementary material Fig. S1). This is comparable to other commercially available sensors (Downing *et al.*, 2012; Khamis *et al.*, 2015) and the range is suitable for monitoring a wide range of natural waters and some engineered systems (e.g. treated effluents and combined sewage overflows). For Peak C the accuracy of calibrated readings was higher when considering the range of values observed during the field deployment (0 - 100 ppb; MAE = 4.42) compared to the full linear range (0 - 1000 ppb; MAE = 9.68). Similarly for Peak T, accuracy was greater for the lower range (0 - 100 ppb; MAE = 2.51) when compared to the full range (0 - 1000 ppb; MAE = 5.51). The minimum detection limit (MDL) was lower for Peak C than Peak T (Table 1) and was comparable to the commercially available sensors tested by Downing *et al.*, (2012) and Khamis *et al.*, (2015).

Temperature correction

Thermal quenching was pronounced for both Peak T and Peak C fluorescence measured using the FL 30 (Fig. 3). The temperature correction algorithm (linear model) was able to adequately compensate for thermal quenching (Fig. 3c & d). The calculated temperature compensation coefficient (ρ) was higher for Peak T (-0.054) than for Peak C (-0.016). This is due to differences in the chemical composition of the fluorophores contributing to Peak T and Peak C fluorescence, particularly the prevalence of the indole group in Peak T compounds which is sensitive to temperature fluctuations (Chen & Barkley, 1998). When comparing ρ values with the literature it is clear that Peak C is comparable with other studies (Table 2). However, ρ for Peak T was greater than that reported by Khamis *et al.* (2015) and Bieroza & Heathwaite (2016) (Table 2). This highlights the importance of determining instrument specific compensation factors before field deployment, particularly for shorter wavelength fluorescence peaks. It is also important to note that the Peak T component was less stable during the experiment. This may be due to light scattering that is more pronounced at short wavelengths, leading to an increase in stray light 'leaking' through the emission filter (Gregory, 2004).

Turbidity effects

In the laboratory suspended particle concentration, measured as turbidity, had a significant effect on the fluorescence signal of the FL30 for both Peak C_{20} and Peak T_{20} (Fig. 4). The response differed between the two peaks and between the sediment size classes (i.e. clay/fine silt, coarse silt and fine sand). Peak C_{20} displayed a linear reduction in fluorescence signal for all sediment types, with OLS slopes ranging from -0.15 to -0.31 for clay/fine silt and fine sand respectively (Fig. 4, Table 3). Signal attenuation at 500 FNU ranged from 70 to 95 %, for clay/silt and fine sand respectively, and was comparable to that observed by Downing *et al.* (2012) for an open path sensors across a similar turbidity range. The Peak T_{20} response varied between sediment types: (i) for clay/fine silt a distinct negative curve linear response with an initial increase followed by a decrease; (ii) for coarse silt a positive curve linear response; (iii) for the fine sand (Bourn Brook sediment) a negative linear response was observed. For clay/fine silt and fine sand a reduction in the fluorescence signal, -50% at 500 FNU, was observed but for very coarse silt (glacial outwash sediment) the signal was amplified by ~+50%. This highlights the need to calibrate sensor output using sediment collected from the field location as particle size, shape and colour exert a strong control on scattering/absorption efficiency, influencing the attenuation and amplification of the fluorescence signal (Gippel, 1995). For Peak T the signal amplification is likely due to a combination of the scattering angle associated with small particles directing excitation light to the emission filter and this stray light leaking through the emission filter Gregory (2005). All turbidity corrections reported herein are based on the Bourn Brook regression coefficients.

Spatial samples and dilution

The DOC (BOD) concentration of samples collected for the dilution tests ranged from 3.7 mg L^{-1} (2.2 mg L^{-1}) to 18.1 mg L^{-1} (95.2 mg L^{-1}) for the Bourn Brook and the STW respectively. When considering all samples and dilutions (n = 22), strong correlations between the FL30 and laboratory spectrofluorometer were observed for Peak C_{20} (r = 0.98) and Peak T_{20} (r = 0.99). For the Peak T_{20} – BOD relationship across the dilution series the Bourn Brook, Canal and Storm Drain were linear and no significant differences in slope or intercept were identified (Fig. 5a; ANOVA; $P > 0.05$). However, for the STW sample non linearity was identified (inspection of linear model residuals) and a 2nd order polynomial fitted the data

(Fig. 5b). Inner filtering was particularly pronounced above BOD 30 mg L^{-1}, a similar threshold was reported by Hudson *et al.,* (2008) for a dilution series of multiple effluent samples. Conversely, for the Peak C_{20} – DOC dilution series, the relationships were linear across the dilution series (Fig. 5c); however, significant differences in slope were identified (ANOVA; $P < 0.05$) with STW displaying a steeper gradient. This is likely due to differences in wastewater DOM composition, particularly the prevalence of protein-like material relative to humic/fulvic like components in wastewater (Carstea *et al.*, 2016) which was highlighted in this study by the T/C ratio (Fig. 5f)

Field data

During the study period mean air temperature was 10.9 ± 3.9 °C (Range = -0.1 – 22.2 °C) and precipitation totalled 109.8 mm (max intensity = 7.0 mm h^{-1}). Mean discharge was 0.16 ± 0.23 $m^3 s^{-1}$ (range = 0.13 – 3.05 $m^3 s^{-1}$). A total of 13 discrete rainfall events were observed, and during four of these events discrete grab samples were collected (see Table S1 for event summary statistics). Storm flow was associated with a dilution in major ion concentrations (i.e. decreased EC), increased particulate load (i.e. increased turbidity) and a dampening of the diurnal water temperature cycle (Fig. 6), although FL 30 measurements were unavailable for 3 days (03/05/15 – 06/05/15) and hence there are no fluorescence data over this period

For the *in-situ* FL30 records, the temperature correction significantly reduced Peak C (9.9 ± 3.1%) and Peak T (28.8 ± 7.4%) as our reference temperature (20 °C) was greater than that observed during spring for the study system. For Peak C_{20} the turbidity correction led to a slight reduction in baseflow readings, however during storm flow conditions when turbidity was elevated a significant increase in readings was apparent. For Peak T_{20} the turbidity correction had little influence on baseflow readings but, as with Peak C_{20}, a distinct signal increase was apparent during high flow conditions (Fig. 6).

Distinct diurnal periodicity was apparent for Peak C_{20} and Peak $C_{20+TURB}$ during days with no precipitation (Fig. S2). Similar patterns were observed by Spencer et al., (2007) for a lowland river and Watras et al., (2015) for a dystrophic lake; and in both cases it was suggested that a combination of photo-degradation and biological activity were driving the oscillation in the Peak C signal. In our study, Peak T broadly tracked the Peak C signal ($r = 0.83$, $P < 0.05$; Fig. 6), and as no diurnal pattern was apparent, it seems that the photodegradation of Peak T may

be less pronounced than Peak C (Moran *et al.*, 2000). However, it is difficult to apportion errors associated with implementing the temperature correction procedure. The relationship between the two peaks has also been explored using laboratory derived results (Fig. S3) and a PARAFAC model showed a strong correlation ($r > 0.9$) between the protein-like component and the Humic UVB component (Khamis unpublished). However, during an extended multi-peak storm event (E_{mp}; Fig. 6) a distinctly higher Peak C signal relative to Peak T was observed during the recession. This suggests the flushing of DOM of increased aromaticity and lower protein content as rainfall intensity fell during the recession phase of the event (Inamdar *et al.*, 2011).

Discrete sampling during storm events

Strong relationships between *in-situ* Peak C_{20}, Peak T_{20} and laboratory measurements of filtered Peak C, Peak T and A_{254} were observed (Fig. 7). The mean Peak T maxima (ex = 283 ± 6.1 nm; em = 361 ± 1.2 nm) was red shifted in comparison to studies on lowland agricultural and woodland catchments (Heinz *et al.*, 2015) while mean Peak C maxima (ex = 353 ± 5.1 nm; em = 432 ± 4.2 nm) was comparable to that observed by other studies from urban river systems (Carstea *et al.*, 2010). *In-situ* corrected Peak $C_{20+Turb}$ and Peak $T_{20+Turb}$ fluorescence were good predictors of DOC (Fig. 8), $R^2 = 0.90$ and $R^2 = 0.90$, respectively. Conversely, for BOD, *in-situ* Peak $C_{20+Turb}$ and Peak $T_{20+Turb}$ were relatively poor predictors (Fig. 9), primarily due to extreme outliers in Event C (high precipitation intensity and turbidity; Table S1). Notably, BOD was positively correlated with turbidity ($R^2 = 0.86$; Fig. 9) suggesting a significant particulate matter contribution to BOD, most probably due to the break-up of biofilms and re-suspension of sediments from storm sewers and the river channel (Volkmar & Dahlgren 2006; Sakrabani *et al.*, 2009). However, the relationship was non-linear and appears to reach an asymptote at ~ 150 FNU (Fig. 9a). The poor relationship between BOD and both Peak T_{20} and Peak $T_{20+TURB}$ during Event C (high precipitation intensity) is of particular interest and is likely due to an increase in either (i) the contribution of non-fluorescent OM to BOD; or (ii) the relative contribution of particulate OM to BOD (Lusk and Toor, 2016). Hence, in this system for turbidity below100 FNU in-situ fluorescence can be used as a reliable BOD surrogate (Table 5)

The LMMs for DOC and BOD are summarised in Tables 4 and 5 respectively. For DOC when all the dataset was used in the LMM the best performing models ($\Delta AICc < 3.0$)

included turbidity as a predictor with either Peak C, Peak C_{20} and Peak T_{20} (Table 4). However, models using laboratory derived turbidity correction factors also performed well; for example Peak $T_{20+TURB}$ + Peak $C_{20+TURB}$ had a marginally higher MAE (0.09 mg L^{-1}) than the best model (Table 4). When the high turbidity data points were removed (> 100 FNU) the best model was comprised of Peak $T_{20+TURB}$ and Peak $C_{20+TURB}$ but improvements associated with the correction coefficients were relatively small as the MAE of single parameter models (Peak C_{20} + 0.04 mg L^{-1}; Peak C +0.1 mg L^{-1}) were relatively low. These findings suggest that empirically derived correction coefficients are suitable for high resolution, continuous DOC monitoring in river systems (Downing *et al.*, 2012; Lee *et al.*, 2015) and if low turbidity is expected a single wavelength Peak C sensor may be used with minimal loss of accuracy (Table 4). For BOD, when considering all data, the best models included turbidity, Peak T_{20}, Peak C_{20} or Peak T (Table 5). Models using laboratory derived turbidity correction factors all performed poorly compared to the data driven regression approaches (MAE > +1.2 mg L^{-1}). When the high turbidity data was removed the best models still included turbidity as a predictor but improvements associated with data driven models were modest compared to Peak $T_{20+TURB}$ (MAE - 0.3 mg L^{-1}). This highlights the need to monitor turbidity alongside Peak T_{20}, even in systems where low turbidity is anticipated, as turbidity interferes with fluorescence measurements (Khamis *et al.*, 2015) but is also indicates particulate load (Lawler *et al.*, 2006). Furthermore, this highlights the need for careful field calibration of fluorescence sensors for monitoring BOD that may involve a period of 'getting to know your systems' with a number of grab samples over a range of hydrological conditions (Sobczak & Raymond, 2015).

CONCLUSIONS

This paper summarises research to develop and test an innovative multi-wavelength fluorescence monitoring system for continuous determinations of BOD and DOC concentration in an urban catchment. The flow-through sensor platform has several advantages in that it can be located on the bankside facilitating maintenance, and it is less expensive than open face, submersible fluorescence sensors. However, it is important to clean the flow-through system regularly, and there are power supply constraints given the need for a peristaltic pump and hence, this system may not be feasible for use in remote locations. In such cases multiple open path sensors, deployed in a multi-parameter sonde or linked to an external data logger, could provide comparable output to the FL30 sensor tested here.

While focusing on a single urban river, this study has highlighted the potential utility of multi-wavelength optical sensing as a tool to probe the OM pool. For monitoring DOC concentration, temperature and turbidity corrected Peak C represent the most cost effective monitoring scenario. A limited improvement in accuracy was achieved with an additional wavelength (i.e. Peak T), however, laboratory derived coefficients, should be based on sediments and matrix water collected from the study site whenever possible. For *in-situ* BOD monitoring a period of 'getting to know your system' is required to build up a field based calibration. This is largely due to the need to quantify the relationship between BOD and both the particulate (turbidity used as a surrogate) and dissolved (fluorescence used as a surrogate) OM fractions. However, where low and relatively stable turbidity is anticipated (i.e. below 100 FNU) adequately compensated fluorescence measurements can provide a continuous indication of BOD. Hence, for accurate monitoring both BOD and DOC concentration a sensor platform monitoring Peak T, Peak C, turbidity and temperature is required.

In-situ fluorescence monitoring represents a cost effective monitoring solution, particularly when compared to UV - absorbance sensors and DOC analysers. Moreover, the approach outlined in this paper has the potential to help address fundamental research questions on urban OM sources, pathways and processing. The sensor also offers the means to increase the temporal resolution of both DOC concentration and BOD monitoring. However, future work should focus on linking *in-situ* fluorescence measurements with: (i) analysis of particulate and soluble fractions of BOD; and, (ii) compositional analysis of the OM pool. This additional information, coupled with longer term monitoring programs, will help to further unravel urban storm water dynamics.

ACKNOWLEDGEMENTS

This research was supported by Innovate UK and is an outcome from a Knowledge Transfer Partnership (KTP) between The University of Birmingham and RS Hydro (KTP no. 9623). The project was co-funded by The Engineering and Physical Sciences Research Council (EPSRC) and The Natural Environment Research Council (NERC). We thank Richard Johnson for logistical support and technical advice regarding installation and sensor calibrations, Pierre Schnegg for sensor communication advice and Eimear Orgill for laboratory support. Detailed and helpful comments provided by two anonymous reviewers significantly improved the manuscript and we are very grateful for their suggestions.

REFERENCES

Aiken G. 2014. Fluorescence and dissolved organic matter: a chemist's perspective. In: Aquatic Organic Matter Fluorescence Edited by PG Coble, J Lead, A Baker, DM Reynolds & RGM Spencer. Cambridge University Press: 35–74.

Baker A. 2004. Protein-like fluorescence intensity as a possible tool for determining river water quality. Hydrological Processes 18: 2927–45. doi:10.1002/hyp.5597

Baker A. 2005. Thermal fluorescence quenching properties of dissolved organic matter. Water Research 39: 4405–12. doi:10.1016/j.watres.2005.08.023

Baker A, Cumberland SA, Bradley C, Buckley C, Bridgeman J. 2015. To what extent can portable fluorescence spectroscopy be used in the real-time assessment of microbial water quality? Science of the Total Environment 532: 14–9. doi:10.1016/j.scitotenv.2015.05.114

Baker A, Elliott S, Lead JR. 2007. Effects of filtration and pH perturbation on freshwater organic matter fluorescence. Chemosphere 67: 2035–43. doi:10.1016/j.chemosphere.2006.11.024

Beggs KMH, Summers RS. 2011. Character and chlorine reactivity of dissolved organic matter from a mountain pine beetle impacted watershed. Environmental Science and Technology 45: 5717–24. doi:10.1021/es1042436

Bieroza MZ, Heathwaite AL. 2015. Seasonal variation in phosphorus concentration–discharge hysteresis inferred from high-frequency in situ monitoring. Journal of Hydrology 524: 333–47. doi:10.1016/j.jhydrol.2015.02.036

Bieroza MZ, Heathwaite AL. 2016. Unravelling organic matter and nutrient biogeochemistry in groundwater-fed rivers under baseflow conditions: Uncertainty in in situ high-frequency analysis. Science of the Total Environment DOI: 10.1016/j.scitotenv.2016.02.046

Burnham KP, Anderson DR. 2002. Model Selection and Multimodel Inference: A Practical Information-Theoretic Approach, Springer: NY.

Carpenter, KD, Kraus, TEC, Goldman, JH, et al. 2013, Sources and characteristics of organic matter in the Clackamas River, Oregon, related to the formation of disinfection by-products in treated drinking water: U.S. Geological Survey Scientific Investigations Report 2013–5001.

Carstea EM, Baker A, Bieroza M, Reynolds D. 2010. Continuous fluorescence excitation-emission

matrix monitoring of river organic matter. Water Research 44: 5356–66. doi:10.1016/j.watres.2010.06.036

Carstea EM, Baker A, Pavelescu G, Boomer I. 2009. Continuous fluorescence assessment of organic matter variability on the Bournbrook River, Birmingham, UK. Hydrological Processes 23: 1937–46. doi:10.1002/hyp

Carstea EM, Bridgeman J, Baker A, Reynolds DM. 2016. Fluorescence spectroscopy for wastewater monitoring: A review. Water Research 95: 205–219 DOI: 10.1016/j.watres.2016.03.021

Cassidy R, Jordan P. 2011. Limitations of instantaneous water quality sampling in surface-water catchments: Comparison with near-continuous phosphorus time-series data. Journal of Hydrology 405: 182–93. doi:10.1016/j.jhydrol.2011.05.020

Chen, Y. and Barkley, MD, 1998. Toward understanding tryptophan fluorescence in proteins. Biochemistry, 37, 9976-9982.

Collins A, Voulvoulis N. 2014. Ecological assessments of surface water bodies at the river basin level: a case study from England. Environmental Monitoring and Assessment 186: 8649–65. doi:10.1007/s10661-014-4033-x

Comber SDW, Gardner MJ, Gunn AM. 1996. Measurement of Absorbance and Fluorescence as Potential Alternatives to Bod. Environmental Technology 17: 771–6. doi:10.1080/09593331708616444

Conmy RN, Del Castillo CE, Downing BD, Chen RF. 2014. Experimental design and quality assurance: in situ fluorescence instrumentation. In: Aquatic Organic Matter Fluorescence Edited by PG Coble, J Lead, A Baker, DM Reynolds & RGM Spencer. Cambridge University Press, 190-230.

Cumberland SA, Bridgeman J, Baker A, Sterling M, Ward D. 2012. Fluorescence spectroscopy as a tool for determining microbial quality in potable water applications. Environmental Technology 33: 687–93.

Downing BD, Pellerin BA, Bergamaschi BA, Saraceno JF, Kraus TEC. 2012. Seeing the light: The effects of particles, dissolved materials, and temperature on in situ measurements of DOM fluorescence in rivers and streams. Limnology and Oceanography: Methods 10: 767–75. doi:10.4319/lom.2012.10.767

Elliott S, Lead JR, Baker A. 2006. Thermal quenching of fluorescence of freshwater, planktonic bacteria. Analytica Chimica Acta 564: 219–25. doi:10.1016/j.aca.2006.01.087

Etheridge JR, Birgand F, Osborne JA, Osburn CL, Burchell MR, Irving J. 2014. Using in situ ultraviolet-visual spectroscopy to measure nitrogen, carbon, phosphorus, and suspended solids concentrations at a high frequency in a brackish tidal marsh. Limnology and Oceanography: Methods 12: 10–22. doi:10.4319/lom.2014.12.10

Fellman JB, D'Amore DV., Hood E, Boone RD. 2008. Fluorescence characteristics and biodegradability of dissolved organic matter in forest and wetland soils from coastal temperate watersheds in southeast Alaska. Biogeochemistry 88 : 169–184. DOI: 10.1007/s10533-008-9203-x

Fellman JB, Hood E, Spencer RGM. 2010. Fluorescence spectroscopy opens new windows into dissolved organic matter dynamics in freshwater ecosystems: A review. Limnology and Oceanography 55: 2452–62. doi:10.4319/lo.2010.55.6.2452

Gippel CJ. 1995. Potential of turbidity monitoring for measuring the transport of suspended solids in streams. Hydrological Processes 9: 83–97.

Goldman, JH, Rounds SA, Needoba JA. 2012. Applications of Fluorescence Spectroscopy for Predicting Percent Wastewater in an Urban Stream. Environmental Science & Technology 46: 4374-4381.

Gregory J. 2004. Particles in Water: Properties and Processes. CRC Press.

Halliday SJ, Skeffington RA, Wade AJ, et al. 2015. High-frequency water quality monitoring in an urban catchment: hydrochemical dynamics, primary production and implications for the Water Framework Directive. Hydrological Processes 29: 3388–407. doi:10.1002/hyp.10453

Heinz M, Graeber D, Zak D, Zwirnmann E, Gelbrecht J, Pusch MT. 2015. Comparison of organic matter composition in agricultural versus forest affected headwaters with special emphasis on organic nitrogen. Environmental Science and Technology 49: 2081–2090 DOI: 10.1021/es505146h

Herschy R. 1985. Stream Flow Measurements. Elsevier Applied Science: Oxford.

Hudson N, Baker A, Ward D, et al. 2008. Can fluorescence spectrometry be used as a surrogate for the Biochemical Oxygen Demand (BOD) test in water quality assessment? An example from South West England. The Science of the Total Environment 391: 149–58. doi:10.1016/j.scitotenv.2007.10.054

Hur, J, Cho J. 2012. Prediction of BOD, COD, and Total Nitrogen Concentrations in a Typical Urban River Using a Fluorescence Excitation-Emission Matrix with PARAFAC and UV Absorption Indices. Sensors 12: 972-986. doi:10.3390/s120100972

Inamdar S, Singh S, Dutta S, et al. 2011. Fluorescence characteristics and sources of dissolved organic matter for stream water during storm events in a forested mid-Atlantic watershed. Journal of Geophysical Research 116: G03043. doi:10.1029/2011JG001735

Jones TD, Chappell NA, Tych W. 2014. First dynamic model of dissolved organic carbon derived directly from high-frequency observations through contiguous storms. Environmental Science & Technology 48: 13289–97.

Jouanneau S, Recoules L, Durand MJ, et al. 2014. Methods for assessing biochemical oxygen demand (BOD): a review. Water research 49: 62–82. doi:10.1016/j.watres.2013.10.066

Kaushal SS, Belt KT. 2012. The urban watershed continuum: evolving spatial and temporal dimensions. Urban Ecosystems 15: 409–35. doi:10.1007/s11252-012-0226-7

Khamis K, Sorensen JPR, Bradley C, Hannah DM, Lapworth DJ, Stevens R. 2015. In situ tryptophan-like fluorometers: assessing turbidity and temperature effects for freshwater applications. Environmental science. Processes & impacts 17: 740–52. doi:10.1039/c5em00030k

Kim JY, Sansalone JJ. 2010. Representation of particulate matter COD in rainfall runoff from paved urban watersheds. Water, Air, and Soil Pollution 205: 113–32. doi:10.1007/s11270-009-0060-6

Lawaetz AJ, Stedmon CA. 2009. Fluorescence intensity calibration using the raman scatter peak of water fluorescence intensity calibration using the raman scatter peak of water. Applied Spectroscopy 63: 936–40.

Lawler DM, Petts GE, Foster IDL, Harper S. 2006. Turbidity dynamics during spring storm events in an urban headwater river system: the Upper Tame, West Midlands, UK. Science of the Total Environment 360: 109–26. doi:10.1016/j.scitotenv.2005.08.032

Lee J, Bang K. 2000. Characterization of urban stormwater runoff. Water Research 34: 1773–80. doi:10.1016/S0043-1354(99)00325-5

Lemke D, Schnegg P-A, Schwientek M, Osenbrück K, Cirpka OA. 2013. On-line fluorometry of multiple reactive and conservative tracers in streams. Environmental Earth Sciences 69: 349–58. doi:10.1007/s12665-013-2305-3

Lusk MG, Toor GS. 2016. Biodegradability and Molecular Composition of Dissolved Organic Nitrogen in Urban Stormwater Runoff and Outflow Water from a Stormwater Retention Pond. Environmental Science & Technology 50: 3391–3398 DOI: 10.1021/acs.est.5b05714

McElmurry SP, Long DT, Voice TC. 2014. Stormwater dissolved organic matter: influence of land cover and environmental factors. Environmental Science & Technology 48: 45–53. doi:10.1021/es402664t

Moran MA, Sheldon WM, Zepp RG. 2000. Carbon loss and optical property changes during long-term photochemical and biological degradation of estuarine dissolved organic matter. Limnology and Oceanography 45 : 1254–1264. DOI: 10.4319/lo.2000.45.6.1254

Moriasi DN, Arnold JG, Liew MW Van, Bingner RL, Harmel RD, Veith TL. 2007. Model evaluation guidelines for systematic quantification of accuracy in watershed simulations. Watershed Simulations 50: 885–900.

Morton D, Rowland C, Wood C, et al. 2011. Final Report for LCM2007 – the new UK Land Cover Map, Lancaster.

Murphy KR, Stedmon CA, Graeber D, Bro R. 2013. Fluorescence spectroscopy and multi-way techniques. PARAFAC. Analytical Methods 5: 6557. doi:10.1039/c3ay41160e

Nakagawa S, Holger S. 2013. A general and simple method for obtaining R^2 from generalized linear mixed-effects models O'Hara RB (ed). Methods in Ecology and Evolution 4: 133–42. doi:10.1111/j.2041-210x.2012.00261.x

Ouattara NK, Garcia-Armisen T, Anzil A, Brion N, Servais P. 2014. Impact of Wastewater Release on the Faecal Contamination of a Small Urban River: The Zenne River in Brussels (Belgium). Water, Air, & Soil Pollution 225: 2043. doi:10.1007/s11270-014-2043-5

Outram FN, Lloyd CEM, Jonczyk J, et al. 2014. High-frequency monitoring of nitrogen and phosphorus response in three rural catchments to the end of the 2011–2012 drought in England. Hydrology and Earth System Sciences 18: 3429–48. doi:10.5194/hess-18-3429-2014

Peacock M, Evans CD, Fenner N, et al. 2014. UV-visible absorbance spectroscopy as a proxy for peatland dissolved organic carbon (DOC) quantity and quality: considerations on wavelength and absorbance degradation. Environmental Science: Processes & Impacts 16: 1445–61. doi:10.1039/c4em00108g

Pellerin BA, Bergamaschi BA, Downing BD, Saraceno JF, Garrett J., Olsen LD. 2013. Optical Techniques for the Determination of Nitrate in Environmental Waters: Guidelines for Instrument Selection, Operation, Deployment, Maintenance, Quality Assurance, and Data Reporting. U.S. Geological Survey Techniques and Methods 1–D5

Pellerin BA, Saraceno JF, Shanley JB, et al. 2011. Taking the pulse of snowmelt: in situ sensors reveal seasonal, event and diurnal patterns of nitrate and dissolved organic matter variability in an upland forest stream. Biogeochemistry 108: 183–98. doi:10.1007/s10533-011-9589-8

R Development Core Team. 2012. R: A language and environment for statistical computing. R Foundation for Statistical Computing, Vienna, Austria. ISBN 3-900051-07-0, URL http://www.R-project.org/.

Sakrabani R, Vollertsen J, Ashley RM, Hvitved-Jacobsen T. 2009. Biodegradability of organic matter associated with sewer sediments during first flush. Science of the Total Environment 407: 2989–95. doi:10.1016/j.scitotenv.2009.01.008

Sandford RC, Bol R, Worsfold PJ. 2010. In situ determination of dissolved organic carbon in freshwaters using a reagentless UV sensor. Journal of Environmental Monitoring 12: 1678–83. doi:10.1039/c0em00060d

Saraceno JF, Pellerin BA, Downing BD, Boss E, Bachand PAM, Bergamaschi BA. 2009. High-frequency in situ optical measurements during a storm event: Assessing relationships between dissolved organic matter, sediment concentrations, and hydrologic processes. Journal of Geophysical Research 114: G00F09. doi:10.1029/2009JG000989

Spencer RGM, Pellerin BA, Bergamaschi BA, et al. 2007. Diurnal variability in riverine dissolved organic matter composition determined by in situ optical measurement in the San Joaquin River (California, USA). Hydrological Processes 21: 3181–9. doi:10.1002/hyp

Strohmeier S, Knorr K-H, Reichert M, et al. 2013. Concentrations and fluxes of dissolved organic carbon in runoff from a forested catchment: insights from high frequency measurements. Biogeosciences 10: 905–16. doi:10.5194/bg-10-905-2013

Sullivan AB, Snyder DM, Rounds SA. 2010. Controls on biochemical oxygen demand in the upper Klamath River, Oregon. Chemical Geology 269: 12–21. doi:10.1016/j.chemgeo.2009.08.007

UKTAG. 2006. UK Environmental Standards and Conditions (Phase 1). WFD UK TAG

Viviano G, Salerno F, Manfredi EC, Polesello S, Valsecchi S, Tartari G. 2014. Surrogate measures for providing high frequency estimates of total phosphorus concentrations in urban watersheds. Water Research 64: 265–77. doi:10.1016/j.watres.2014.07.009

Volkmar EC, Dahlgren RA. 2006. Biological oxygen demand dynamics in the lower San Joaquin River, California. Environmental Science and Technology 40: 5653–60. doi:10.1021/es0525399

Wade AJ, Palmer-Felgate EJ, Halliday SJ, et al. 2012. Hydrochemical processes in lowland rivers: insights from in situ, high-resolution monitoring. Hydrology and Earth System Sciences 16: 4323–42. doi:10.5194/hess-16-4323-2012

Watras CJ, Hanson PC, Stacy TL, et al. 2011. A temperature compensation method for CDOM fluorescence sensors in freshwater. Limnology and Oceanography: Methods 9: 296–301. doi:10.4319/lom.2011.9.296

Watras CJ, Morrison K a., Crawford JT, McDonald CP, Oliver SK, Hanson PC. 2015. Diel cycles in the fluorescence of dissolved organic matter in dystrophic Wisconsin seepage lakes: Implications for carbon turnover. Limnology and Oceanography 60: 482–96. doi:10.1002/lno.10026

Xu Z, Xu YJ. 2015. Rapid field estimation of biochemical oxygen demand in a subtropical eutrophic urban lake with chlorophyll a fluorescence. Environmental Monitoring and Assessment 187: 4171. doi:10.1007/s10661-014-4171-1

Yamashita Y, Tanoue E. 2003. Chemical characterization of protein-like fluorophores in DOM in relation to aromatic amino acids. Marine Chemistry 82: 255–71. doi:10.1016/S0304-4203(03)00073-2

Yang L, Shin H-S, Hur J. 2014. Estimating the concentration and biodegradability of organic matter in 22 wastewater treatment plants using fluorescence excitation emission matrices and parallel factor analysis. Sensors 14: 1771–86. doi:10.3390/s14010177

Table 1. Instrumentation used for *in-situ* measurements. For the GGNU-FL30 MDL minimum detection limit and precision were determined as in Khamis *et al.*, (2015), linear range was determined by comparing the slope of regression model for increasing ranges and the linear range determined as the point at which the slope was significantly different from 1.

Parameter	Instrument	Specification
Water Level	PDCR-830 (GE, Fairfield, USA) Vented pressure sensor	Accuracy ± 0.6% of reading
Electrical Conductivity	CS54A7 (Campbell Scientific, Logan, USA) - Potentiometric Electrode	Accuracy ± 5% of reading
Temperature	CS54A7 – Thermistor	Accuracy ± 0.4°C
Turbidity	GGUN - FL30	MDL = 0.8 NTU
	660nm - detector 90° scatter	linear range = 0 – 1000 NTU
		Precision across range = 1.9%
Peak T	GGUN - FL30	MDL = 1.74 ppb
	Ex 285nm ± 12 nm (FWHM)	linear range = 0 – 1000 ppb
	Em 345 ± 25 nm (FWHM)	Precision across range = 2.5%
Peak C	GGUN - FL30	MDL = 1.39 ppb
	Ex 365nm ± 15 nm (FWHM)	linear range = 0 – 1000 ppb
	Em 490 ± 30 nm (FWHM)	Precision across range = 0.7%

Table 2. Temperature compensation coefficients (ρ) estimated for this study and compared with other studies. The reference temperature for all studies was 20°C. NOM*= Suwannee NOM (IHSS aquatic reference material); NOM^= Pahokee soil (IHSS aquatic reference material);QS = Quinine Sulphate.

Study	Fluorescence peak (Sensor)	Matrix	Temperature coefficient (mean ± SD)
This study	C (FL30)	River water	-0.016 ± 0.0007
	T (FL 30)	River water	-0.054 ± 0.008
Khamis *et al.* (2015)	T (Turner –Cyclops 7)	L-Tryptophan	-0.039 ± 0.0145
	T (Chelsea UV Lux)	L -Tryptophan	-0.049 ± 0.0134
Bieroza & Heathwaite (2016)	T (Chelsea UV Lux)	L -Tryptophan	-0.020 ± na
Downing *et al.* (2012)	C (multiple model)	NOM*^ & QS^	-0.012 ± 0.004
Watras *et al.* (2011)	C (Turner –Cyclops 7)	Lake water	-0.098 ± 0.001
	C (Sea Point)	Lake water	-0.016 ± 0.002
	C (Sea Point)	NOM*	-0.026 ± 0.003
Lee *et al.* (2015)	C (Turner –Cyclops 7)	River water	-0.017 ± 0.004

Table 3. Regression coefficients for the turbidity correction models. Where a 2nd order polynomial model was deemed to have the best fit (lower AIC score than the linear model) the coefficient is displayed in the Turbidity^2 column. Non-significant parameters are marked ^{ns} all other parameters are significant at $\alpha = 0.999$.

Sediment	Fluorescence peak	Intercept	Turbidity	**Turbidity^2**
Clay	C_{20}	-1.58 ± 0.45	-0.15 ± 0.001	-
	T_{20}	0.08 ± 0.87^{ns}	0.12 ± 0.005	-3.81e^{-4} ± 1.57e^{-5}
Silt	C_{20}	-2.51 ± 0.51	-0.14 ± 0.002	-
	T_{20}	-4.13 ± 1.0	-0.31 ± 0.01	-4.45e-^{4} ± 2.70e^{-5}
Bourn Brook	C_{20}	6.1± 1.54	-0.23 ± 0.05	-
	T_{20}	-7.45 ± 1.22	-0.11 ± 0.02	-

Table 4. Mixed effect model results testing the relationship between in-situ optical measurements (Peak T, Peak C and turbidity) and laboratory DOC determinations. Models are ranked by AICc scores in addition models are benched marked by mean absolute error (MAE) and percent bias (% bias). All models are significant at $P < 0.05$ and have a random intercept term of sample time nested in sample event.

DOC (all data)						DOC (> 100 FNU removed)					
Model variables	**R^2**	**AICc**	**ΔAICc**	**MAE**	**% Bias**	**Model variables**	**R^2**	**AICc**	**ΔAICc**	**MAE**	**% Bias**
TURB + Peak C_{20}	0.96	85.3	0	0.56	-0.9	Peak $T_{20+TURB}$ + Peak $C_{20+TURB}$	0.98	58.2	0	0.37	-0.1
TURB + Peak T_{20} + Peak C_{20}	0.96	85.9	0.6	0.57	-0.7	Peak $C_{20+TURB}$	0.98	61.1	2.9	0.43	-0.6
TURB + Peak C	0.95	87.5	2.2	0.62	-1.2	TURB + Peak T_{20} + Peak C_{20}	0.98	63	4.8	0.4	-0.1
TURB + Peak T + Peak C	0.96	88.9	3.6	0.62	-1	TURB + Peak C_{20}	0.98	64.2	6	0.44	-0.5
TURB + Peak T_{20}	0.93	98.2	12.9	0.8	-0.4	Peak C_{20}	0.97	68.2	10	0.41	-0.1
TURB + Peak T	0.93	98.9	13.6	0.77	-0.6	TURB + Peak C	0.97	68.4	10.2	0.52	-0.9
Peak $T_{20+TURB}$ + Peak $C_{20+TURB}$	0.92	106.3	21	0.65	-1.1	Peak T_{20} + Peak C_{20}	0.97	68.9	10.7	0.45	0.1
Peak $C_{20+TURB}$	0.90	107.8	22.5	0.73	-1.6	TURB + Peak T + Peak C	0.97	69.3	11.1	0.49	-0.5
Peak $T_{20+TURB}$	0.90	108	22.7	0.81	-1	Peak C	0.97	71.2	13	0.47	-0.3
Peak C	0.86	120.5	35.2	1	-2.1	Peak T + Peak C	0.97	72.3	14.1	0.52	-0.1
Peak C_{20}	0.86	120.7	35.4	0.93	-2	TURB + Peak T_{20}	0.96	76.1	17.9	0.54	0
Peak T	0.86	120.8	35.5	1.12	-1.2	Peak $T_{20+TURB}$	0.96	76.7	18.5	0.74	0.9
Peak T + Peak C	0.87	120.8	35.5	1.03	-1.6	TURB + Peak T	0.96	79.7	21.5	0.6	-0.2
Peak T_{20} + Peak C_{20}	0.87	121.5	36.2	0.99	-1.7	Peak T	0.94	87.5	29.3	0.96	0.9
Peak T_{20}	0.85	122.8	37.5	1.23	-1.4	Peak T_{20}	0.94	88.1	29.9	1.13	1.9
TURB	0.55	159.9	74.6	2.79	-9.1	TURB	0.85	111.9	53.7	1.47	-7.6

Table 5. Mixed effect model results testing the relationship between in-situ optical measurements (Peak T, Peak C and turbidity) and laboratory BOD determinations. Models are ranked by AICc scores with R^2 ,mean absolute error (MAE), percent bias (% bias) also displayed. All models are significant at $P < 0.05$ and have a random intercept term of sample time nested in sample event.

BOD (all data)						BOD (> 100 FNU removed)					
Model variables	**R^2**	**AICc**	**ΔAICc**	**MAE**	**% Bias**	**Model variables**	**R^2**	**AICc**	**ΔAICc**	**MAE**	**% Bias**
TURB + Peak T_{20}	0.95	89.8	0	0.56	0	TURB + Peak T + Peak C	0.96	55.7	0	0.36	-0.2
TURB + Peak T_{20} + Peak C_{20}	0.95	91.3	1.5	0.56	0	TURB + Peak T	0.94	59.4	3.7	0.41	0
TURB + Peak T	0.94	92.3	2.5	0.51	0	TURB + Peak T_{20}	0.94	61.8	6.1	0.43	0.1
TURB + Peak T + Peak C	0.94	95.3	5.5	0.5	0	TURB + Peak T_{20} + Peak C_{20}	0.94	62.2	6.5	0.4	0
TURB + Peak C_{20}	0.93	97.6	7.8	0.6	0	TURB + Peak C	0.91	70.1	14.4	0.49	-0.1
TURB + Peak C	0.93	98	8.2	0.59	0	TURB + Peak C_{20}	0.91	70.4	14.7	0.49	-0.1
TURB	0.86	115.7	25.9	1.01	-1.6	TURB	0.88	76.2	20.5	0.62	-1.7
Peak $T_{20+TURB}$	0.57	155.8	66	1.85	-1.2	Peak $T_{20+TURB}$	0.85	81.4	25.7	0.67	1.4
Peak $T_{20+TURB}$ + Peak $C_{20+TURB}$	0.60	156.2	66.4	1.93	-0.1	Peak $C_{20+TURB}$	0.85	81.6	25.9	0.64	0.2
Peak $C_{20+TURB}$	0.52	160.2	70.4	1.83	-3.3	Peak $T_{20+TURB}$ + Peak $C_{20+TURB}$	0.86	82.7	27	0.64	0.6
Peak T_{20}	0.51	160.9	71.1	1.97	-2.7	Peak T	0.84	84	28.3	0.66	1.3
Peak T	0.50	161.6	71.8	1.96	-2.4	Peak C	0.83	85.6	29.9	0.66	0.2
Peak T_{20} + Peak C_{20}	0.53	161.8	72	2.07	-2	Peak T + Peak C	0.84	86.1	30.4	0.63	0.8
Peak T + Peak C	0.51	163.5	73.7	2.01	-1.4	Peak T_{20}	0.82	87	31.3	0.69	0.2
Peak C_{20}	0.46	163.7	73.9	1.95	-4.3	Peak C_{20}	0.81	88.5	32.8	0.77	1.7
Peak C	0.46	163.9	74.1	1.94	-4.3	Peak T_{20} + Peak C_{20}	0.82	89.1	33.4	0.7	0.6

Figure 1. (a) FL30 optical setup. (b) The peaks measured by the FL30; Peak C (UVA Humic like fluorescence) and Peak T (Tryptophan-like fluorescence) highlighted in the wider EEM. The red boxes represent the FMHW of the sensor measurement window. The EEM displayed is a sample collected directly downstream of a small sewage treatment works, Worcestershire, UK.

Figure 2. (a) Map of the UK with study region highlighted. (b) Location of study catchment (red) in the West Midlands. Urban areas (grey), woodland (green) and the river network (blue) are also highlighted (c) land use map for the Bourn Brook catchment with sample location and meteorological site highlighted.

Figure 3. Temperature quenching of Peak C (a) and Peak T (b) for 4 dilutions (1, 0.75, 0.5, 0.25) of Bourn Brook stream water. Temperature corrected data for Peak C (c) and Peak T (d) are displayed.

Figure 4. Change in the FL30 fluorescence signal (Peak C and T) of Bourn Brook waters in response to changing turbidity. (a) Response curves for a clay sediment (D_{50} = 11.9 µm); (b) Response curves for a silt sediment (D_{50} = 52.1 µm) (c) Response curves for Bourn Brook sediment (D_{50} = 82.1 µm)**.**

Figure 5. (a) BOD dilution series for samples collected from the Bourn Brook (BBR), Birmingham Canal, and a storm drain. No significant differences in slope or intercept were identified (ANOVA; $P > 0.05$); (b) BOD dilution series for a sewage treatment works (primary effluent; STW); note that inner filtering was apparent and is particularly pronounced at BOD >30 mg L^{-1} /12.5 (RFU). (c) DOC dilution for all samples; note all were linear across the dilution series, however significant differences in slope were identified (ANOVA; $P < 0.05$). (d) Sample dilution vs Peak T_{20} fluorescence. Linear responses observed for all samples except STW which suggested inner filtering occurred at > 75%. (e) Sample dilution vs Peak C_{20}. (f) Ratio of Peak T/ Peak C for each sample error bars represent 95% CI for the dilution series (n = 5).

Figure 6. *In-situ* variables recorded at the Bourn Brook test site (08/04/2015-20/06/2015). Upper panel displays discharge, precipitation and water temperature (Tw), the middle panels display Peak T and Peak C respectively. The lower panel displays electrical conductivity (EC) and turbidity. The four events when discrete sampling was undertaken for laboratory analysis are labelled A-D, further event of interest.

Figure 7. Scatterplot matrix displaying the relationship between in-situ and laboratory measured parameters. The red line is a LOESS smoother (span = 0.7).

Figure 8. Relationship between DOC concentration and a) turbidity, b) absorbance at 254nm , c) Peak C corrected for temperature, d) Peak T corrected for temperature, e) Peak C corrected for temperature and turbidity, and f) Peak T corrected for temperature and turbidity. NB Italics denotes laboratory measurement (i.e. absorbance 254nm) and lines of best fit are only displayed if $P < 0.1$.

Figure 9. Relationship between BOD concentration and a) turbidity, b) absorbance at 254nm, c) Peak C corrected for temperature, d) Peak T corrected for temperature, e) Peak C corrected for temperature and turbidity, and f) Peak T corrected for temperature and turbidity. Italics denotes laboratory measurement (i.e. absorbance 254nm) and lines of best fit are only displayed if $P < 0.1$.

Figure 1.

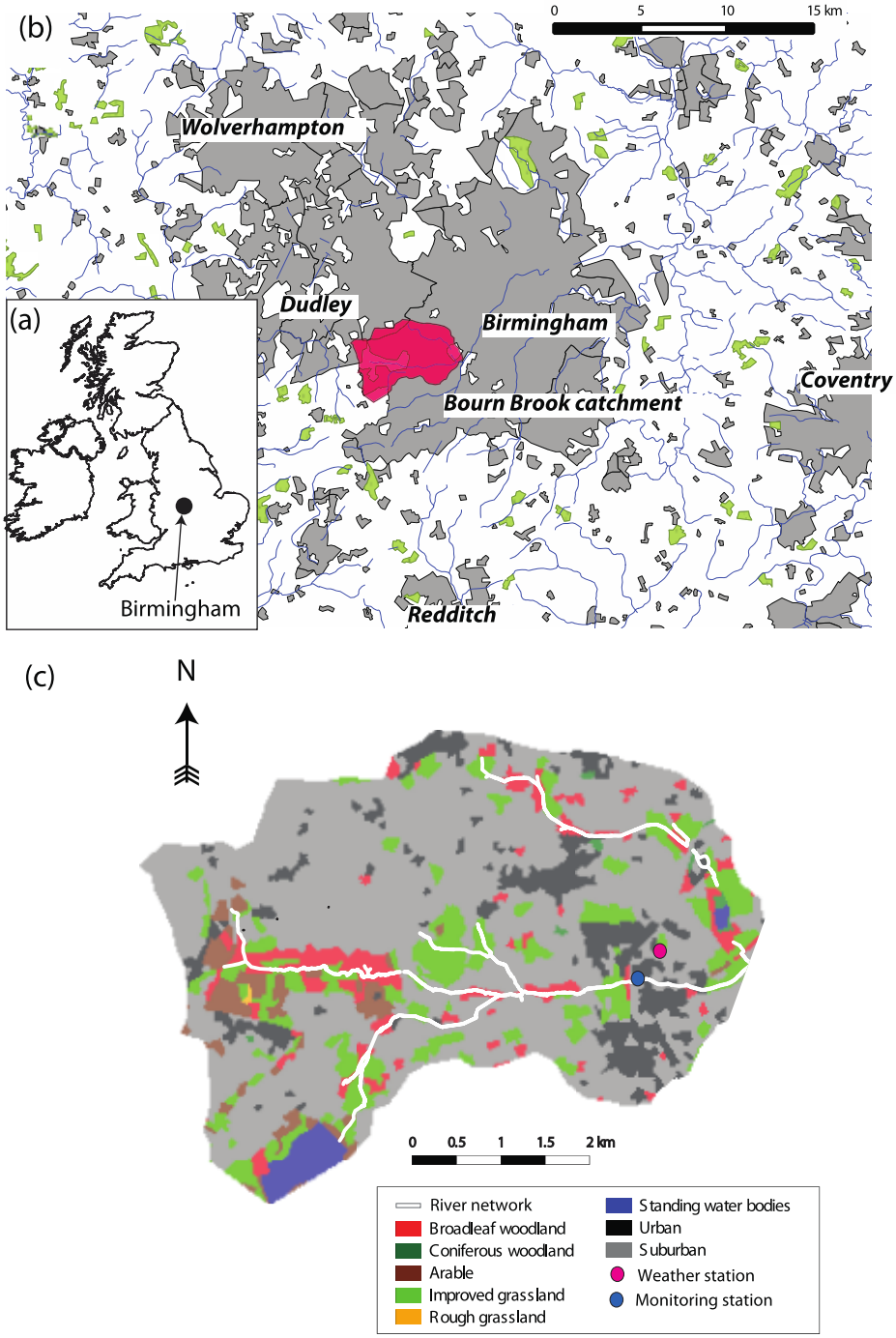
(b)
0 5 10 15 km
Wolverhampton
Dudley
Birmingham
Coventry
Bourn Brook catchment
Redditch
(a)
Birmingham
(c)
N
0 0.5 1 1.5 2 km
River network
Broadleaf woodland
Coniferous woodland
Arable
Improved grassland
Rough grassland
Standing water bodies
Urban
Suburban
Weather station
Monitoring station

Figure 2.

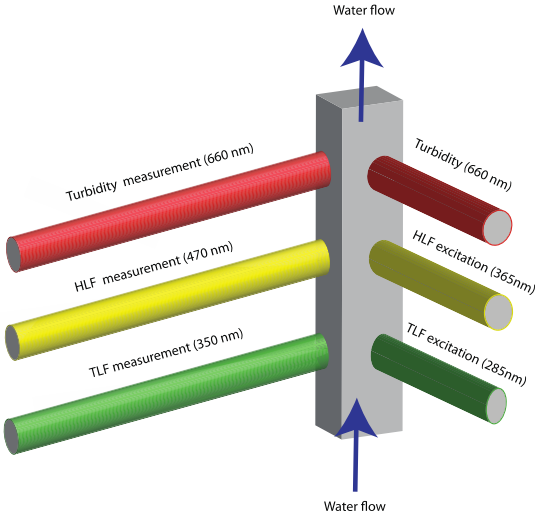
Water flow
Turbidity measurement (660 nm)
HLF measurement (470 nm)
TLF measurement (350 nm)
Turbidity (660 nm)
HLF excitation (365nm)
TLF excitation (285nm)
Water flow

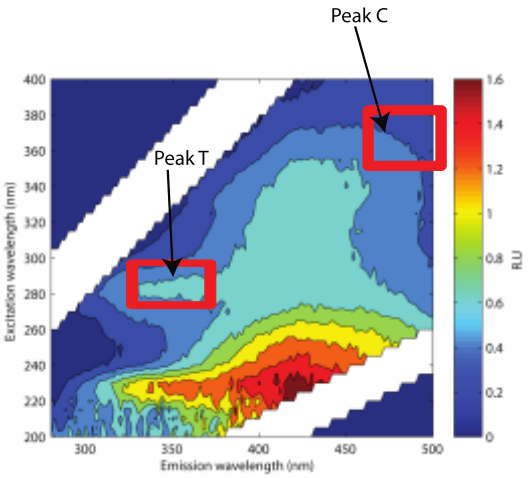
Peak C
Peak T
Excitation wavelength (nm)
Emission wavelength (nm)
R.U

Figure 3.

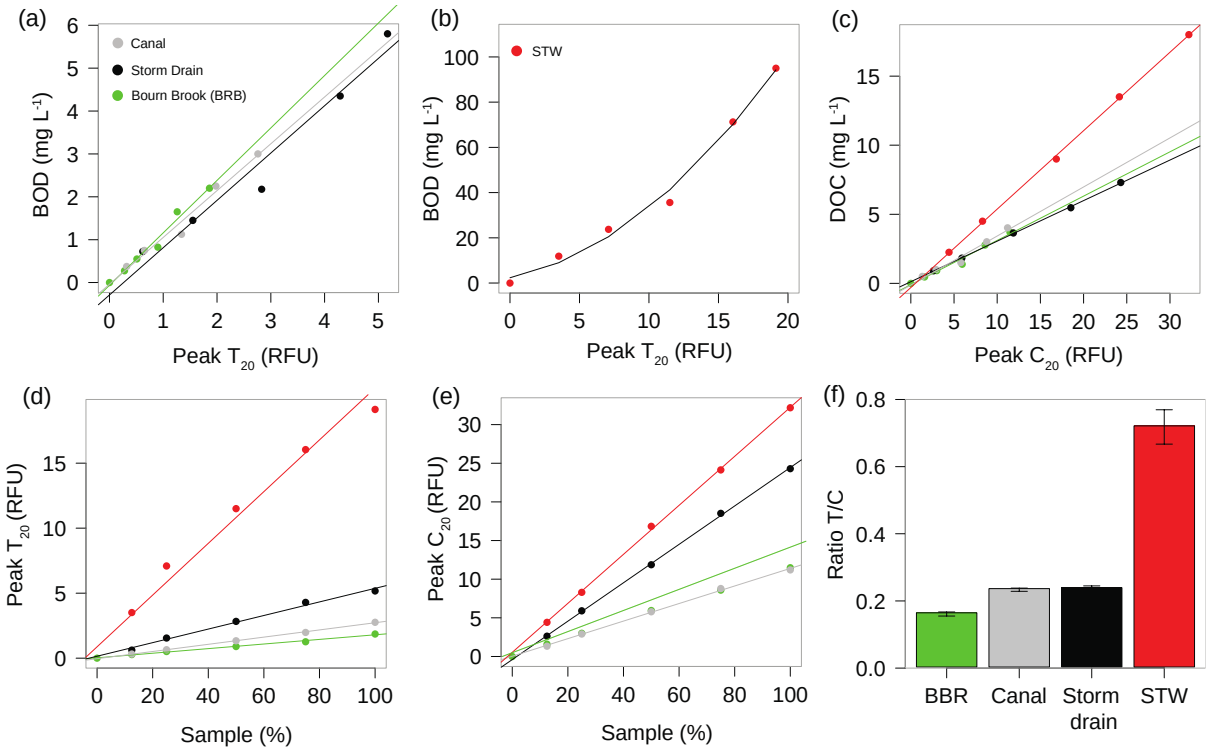
(a)
Canal
Storm Drain
Bourn Brook (BRB)
BOD (mg L-1)
Peak T20 (RFU)
(b)
STW
BOD (mg L-1)
Peak T20 (RFU)
(c)
DOC (mg L-1)
Peak C20 (RFU)
(d)
Peak T20 (RFU)
Sample (%)
(e)
Peak C20 (RFU)
Sample (%)
(f)
Ratio T/C
BBR
Canal
Storm drain
STW

Figure 4.

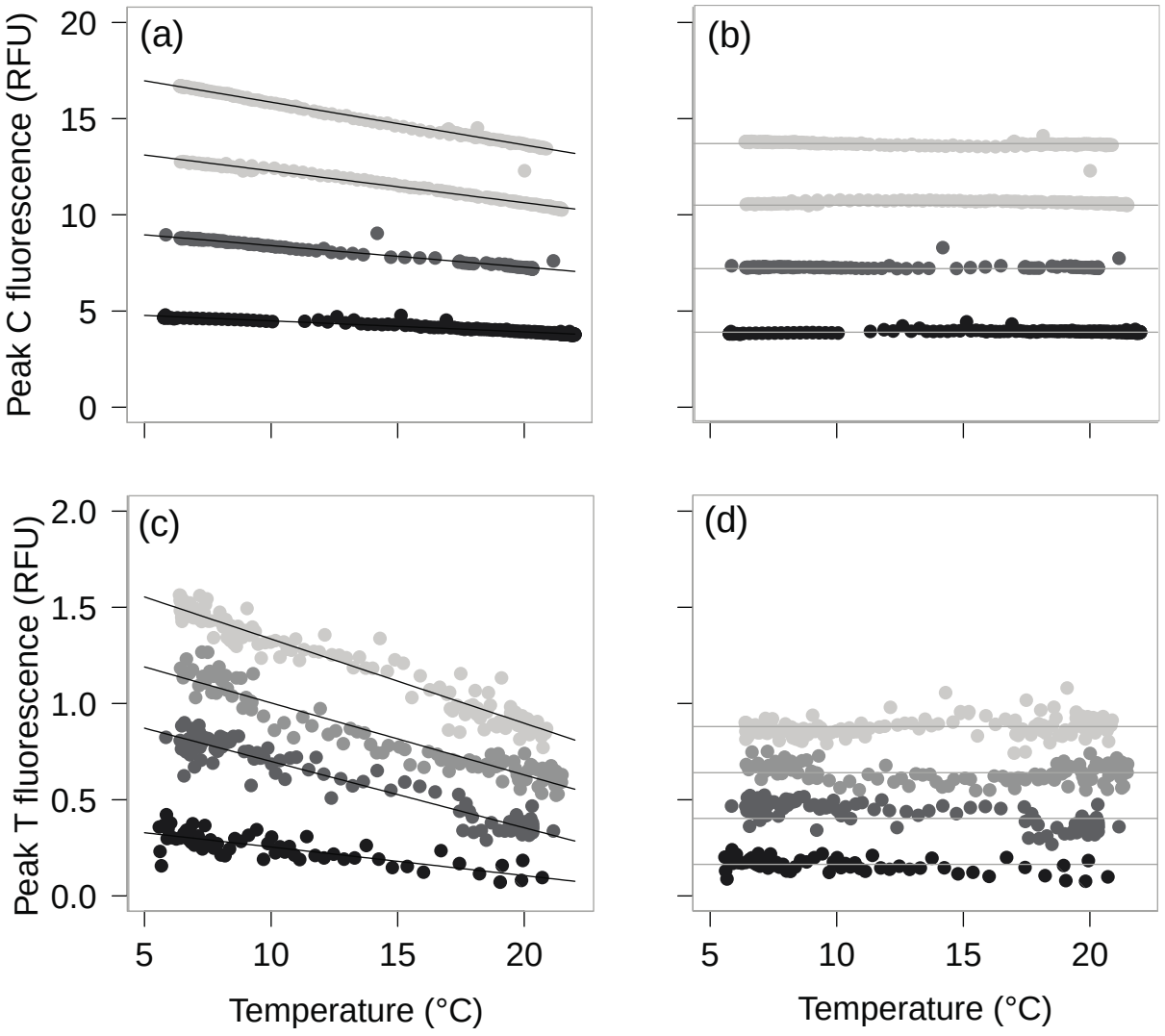
(a)
(b)
(c)
(d)
Peak C fluorescence (RFU)
Peak T fluorescence (RFU)
Temperature (°C)
Temperature (°C)
0
5
10
15
20
0.0
0.5
1.0
1.5
2.0
5
10
15
20

Figure 5.

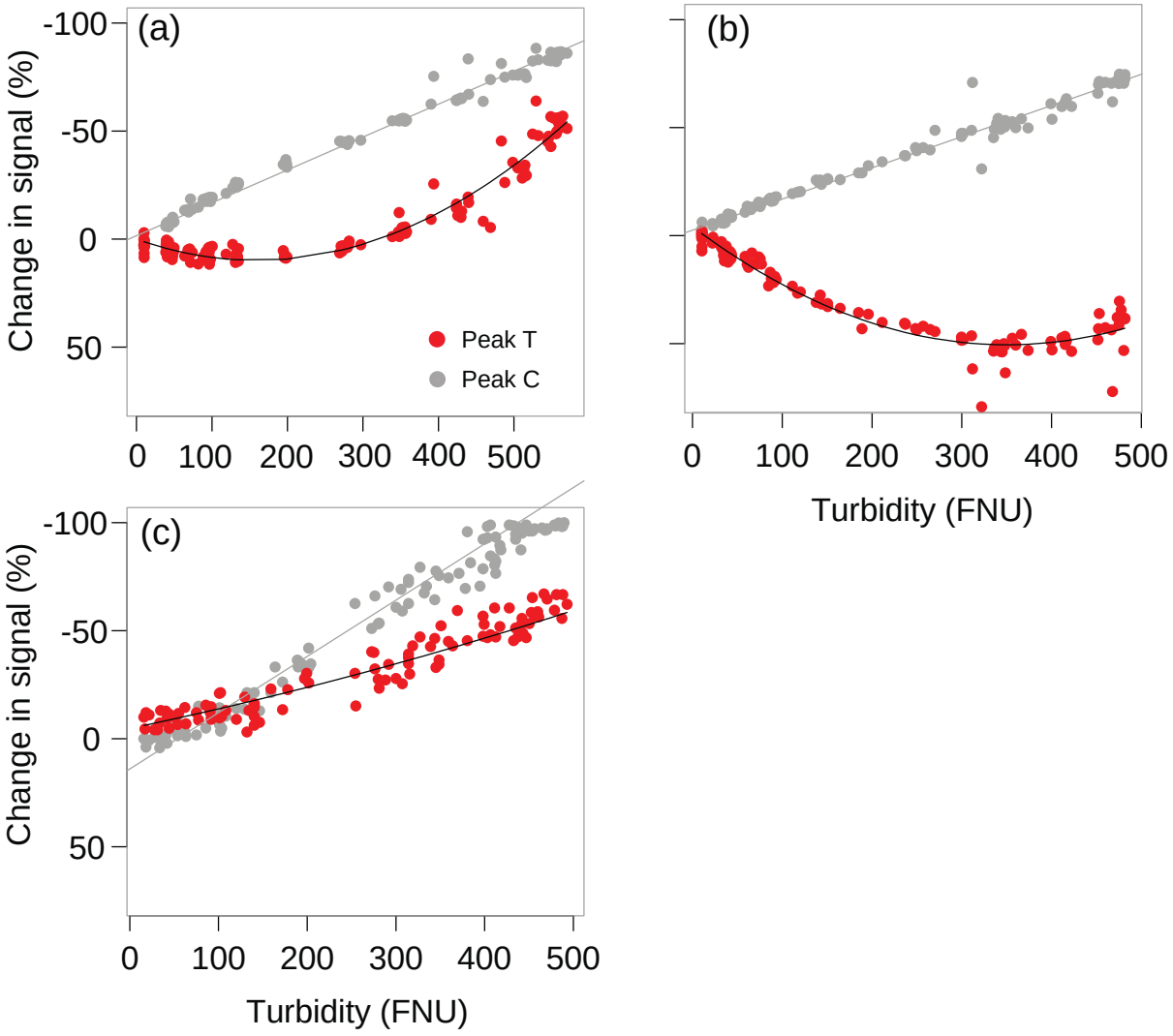
(a)
(b)
(c)
Change in signal (%)
-100
-50
0
50
Peak T
Peak C
0
100
200
300
400
500
Turbidity (FNU)

Figure 6.

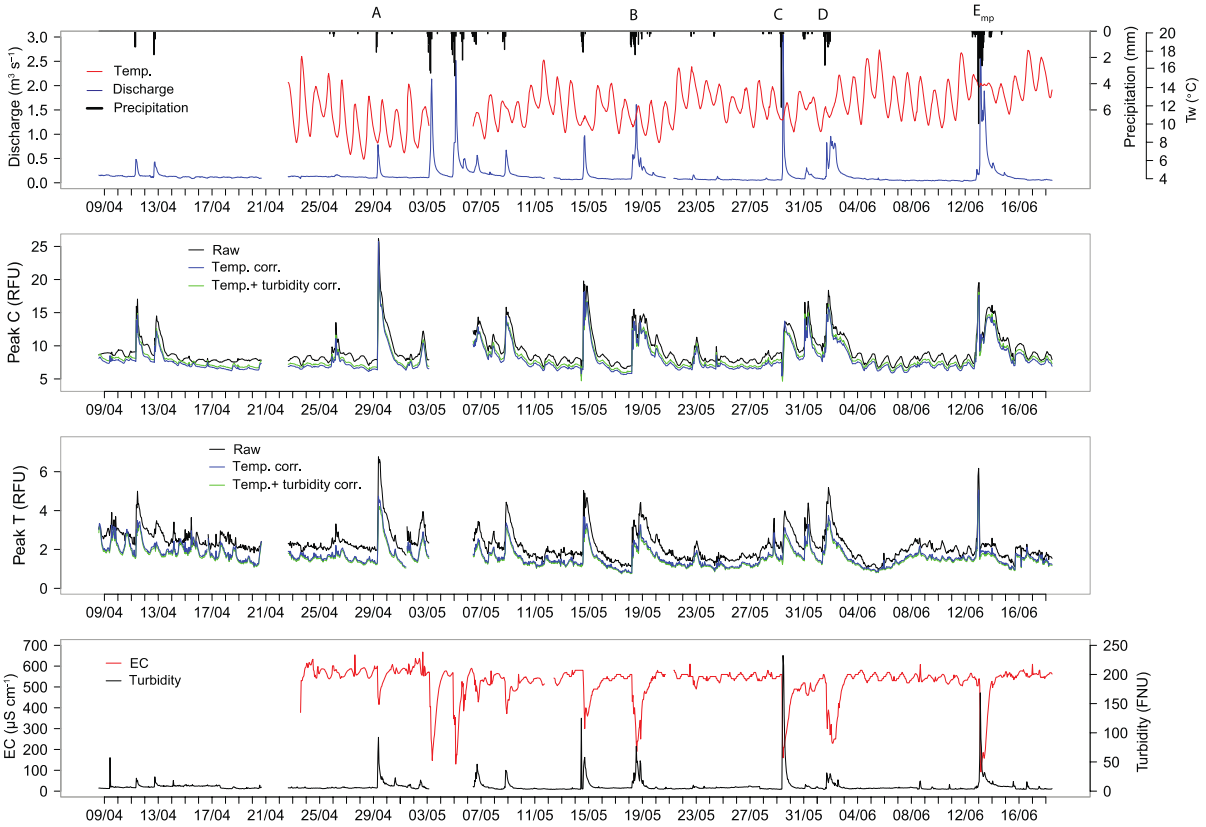
A
B
C
D
E_mp
Discharge (m³ s⁻¹)
Temp.
Discharge
Precipitation
Precipitation (mm)
Tw (°C)
Peak C (RFU)
Raw
Temp. corr.
Temp.+ turbidity corr.
Peak T (RFU)
EC (µS cm⁻¹)
EC
Turbidity
Turbidity (FNU)
09/04 13/04 17/04 21/04 25/04 29/04 03/05 07/05 11/05 15/05 19/05 23/05 27/05 31/05 04/06 08/06 12/06 16/06

Figure 7.

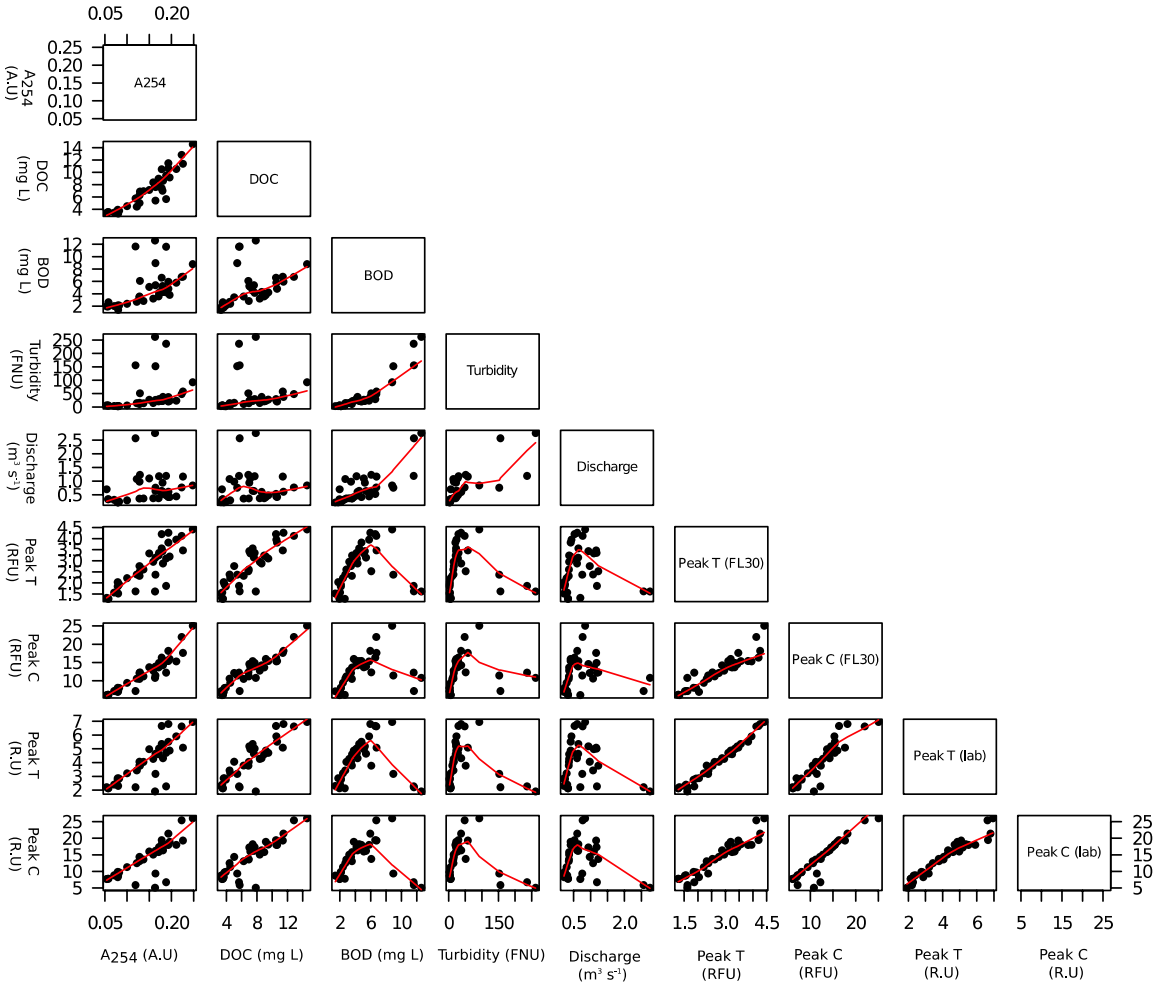
A254
DOC
BOD
Turbidity
Discharge
Peak T (FL30)
Peak C (FL30)
Peak T (lab)
Peak C (lab)
A254 (A.U)
DOC (mg L)
BOD (mg L)
Turbidity (FNU)
Discharge (m³ s⁻¹)
Peak T (RFU)
Peak C (RFU)
Peak T (R.U)
Peak C (R.U)

Figure 8.

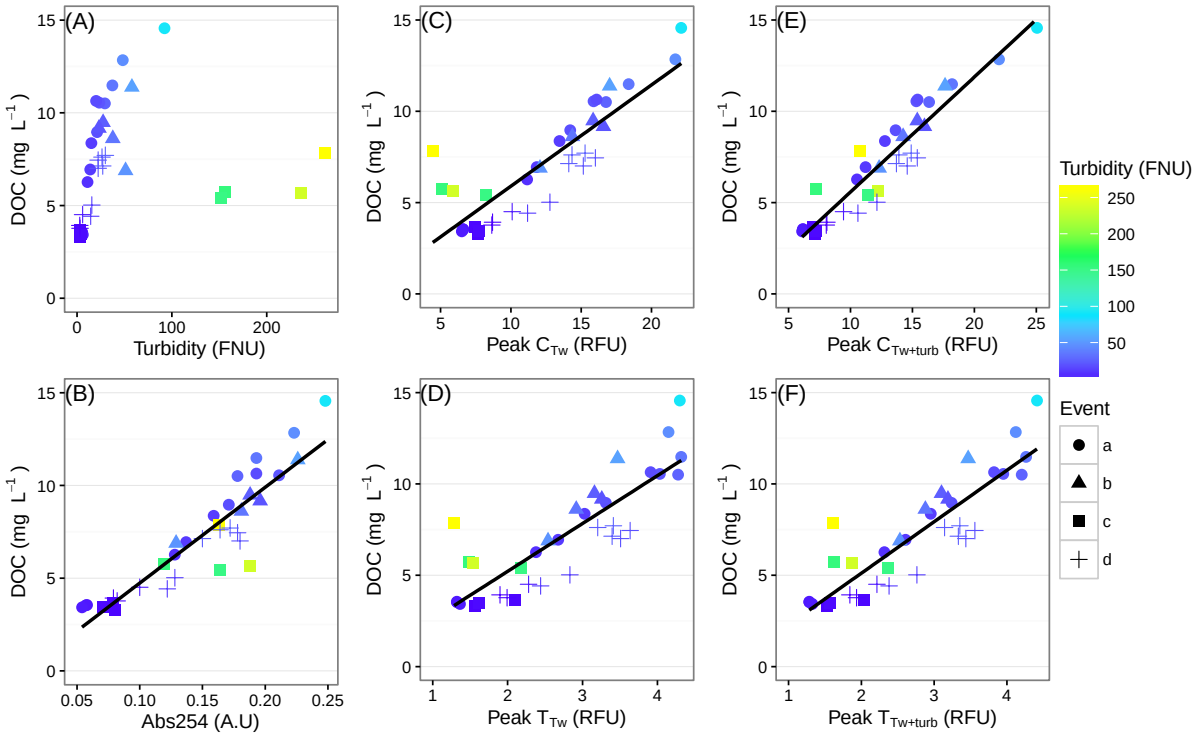
(A)
(B)
(C)
(D)
(E)
(F)
DOC (mg L^{-1})
Turbidity (FNU)
Abs254 (A.U)
Peak C_{Tw} (RFU)
Peak T_{Tw} (RFU)
Peak $C_{Tw+turb}$ (RFU)
Peak $T_{Tw+turb}$ (RFU)
Turbidity (FNU)
250
200
150
100
50
Event
a
b
c
d

Figure 9.

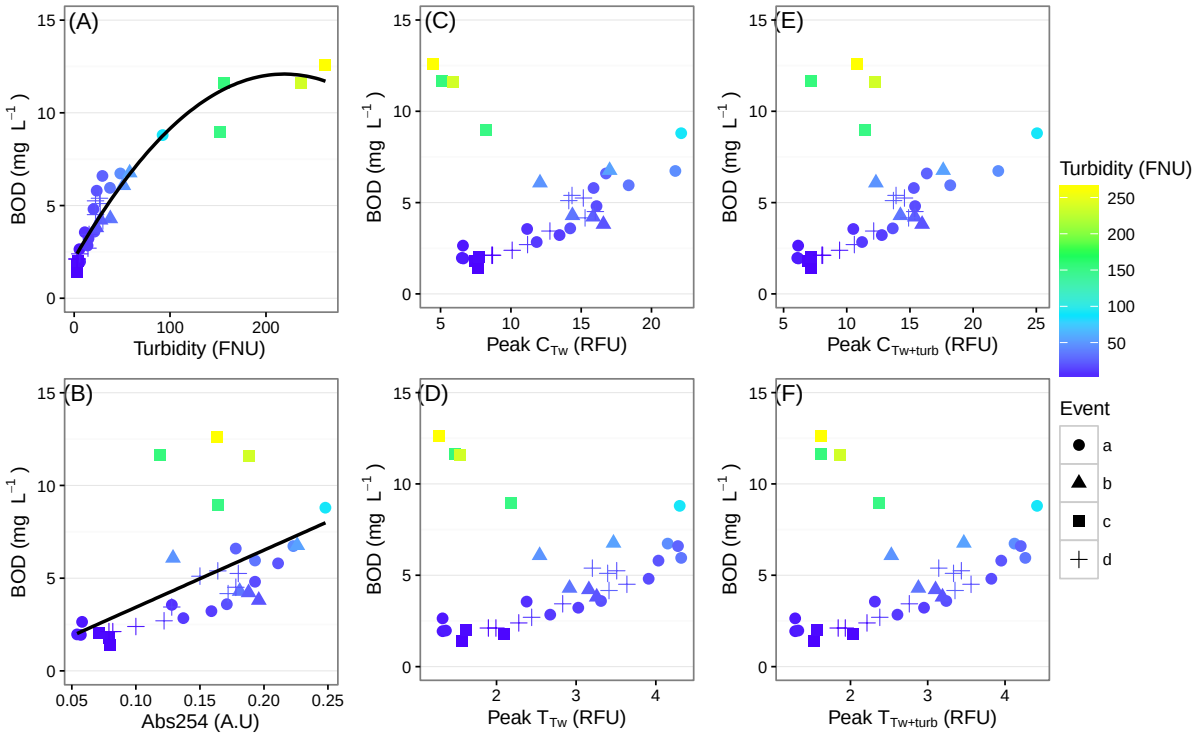
(A)
(B)
(C)
(D)
(E)
(F)
BOD (mg L^{-1})
Turbidity (FNU)
Abs254 (A.U)
Peak C_{Tw} (RFU)
Peak T_{Tw} (RFU)
Peak $C_{Tw+turb}$ (RFU)
Peak $T_{Tw+turb}$ (RFU)
Turbidity (FNU)
250
200
150
100
50
Event
a
b
c
d